Original Article

Evaluation of the influence of low Mg content on the mechanical and microstructural properties of β titanium alloy

Mariana Correa Rossi [a,*], Daniel Leal Bayerlein [b], Eber de Santi Gouvêa [a],
Montserrat Vicenta Haro Rodríguez [a], Angel Vicente Escuder [a],
Vicente Amigó Borrás [a]

[a] Universitat Politècnica de València, Institut de Tecnologia de Materials, Camí de Vera S/n, València, 46022, Spain
[b] Instituto de Pesquisas Energéticas e Nucleares, Centro de Ciência e Tecnologia de Materiais, Av. Prof. Almeida Prado 532 Cid, Universitária - Butantã, São Paulo, 05508-901, Brazil

ARTICLE INFO

ABSTRACT

It was investigated in order to better understand the relationship between the low presence of Mg in the Ti—Nb—Sn alloy in its mechanical and microstructural properties by the powder metallurgy technique for biomedical application. The blended powders with the nominal composition of Ti—34Nb—6Sn were obtained by milling at 200 rpm/40 min, compacted at 200 MPa. The sintering were carried out at 900 °C/2 h and at 1110 °C/2 h, followed by furnace cooling. The particle size was characterized by the dynamic image analyzer (DIA). The phases quantification and their microstructure were characterized by an X-ray diffractometer (XRD) and a scanning electron microscope (SEM). The porosity was characterized by the Archimedes method and also bi-dimensionally by the Image J software. The mechanical tests were performed by the impulse excitation (Sonelastic ®) technique, in order to evaluate the elastic modulus (E) of the sintered materials and the hardness and resistance by the Rockwell method. The results indicated that the sintering at 1100 °C in the materials with Mg, still had particles of Nb not diffused. The microstructure was basically formed by two phases with the presence of Nb non-diffused in all conditions except at 1100 °C in the system without Mg. The β phase % for systems without and with Mg at 900 °C was approximately 80% and 65%. At 1100 °C, 76% and 78%. The E and hardness were 31 GPa and 226 MPa at 900 °C; 49 GPa and 344 MPa at 1100 °C for materials with Mg. The O and N content increased approximately 1.3 times when adding Mg powder.

---

* Corresponding author.
E-mail address: mrncorrea90@gmail.com (M.C. Rossi).

1.   Introduction

The metallic materials, in general, present a set of excellent mechanical characteristics, in which the ceramic and polymeric materials do not have. These characteristics can be modified, increasing or decreasing them depending on the processing technique. With the increase in life expectancy of the world population, as well as the high rate of traffic accidents, the number of medical devices has increased significantly. The orthopedic market, that include the endoprostheses, only in U.S is estimated more than US$ 4 billion in the year 2020 [1]. This condition becomes necessary not only for the production of these devices, but for improvements in their synthesis, since many materials do not have certain characteristics that are biocompatible for a long time. Materials that include non-toxic elements, such as Nb and Sn in Ti alloys, are excellent options for the development of new biomedical devices [2] besides not being harmful to the body, Nb as β phase stabilizing element in certain% lower elastic modulus [2,3], which is another parameter that contributes to the low durability of orthopedic prostheses. The elastic module, when very discrepant from bone tissue, causes the tissue around the implant to be discouraged over time due to the almost total absorption of mechanical stress by the prosthesis. This characteristic is due to the fact that the elastic modulus of these materials is significantly superior to that of bone [4]. Thus, one option is the production of materials with a high percentage of β phase, which provides better mechanical compatibility. In addition, the mechanical characteristics are directly related to the type of microstructure formed after processing the materials. In titanium alloys, the main barrier to the displacement movement is represented by the β/α interfaces, thus, referring to the α phase morphology and distribution, which normally delineate the mechanical resistance of the alloys [5]. The Ti—30Nb—4Sn alloy studied by Mahran and Omran showed good mechanical properties of hardness, but still with high elastic modulus [6]. Other alloys like Ti—16Sn—4Nb [7], Ti—30Nb—5Sn [8] and Ti—25Nb—11Sn [9] showed adequate results of hardness, but the elastic modulus was not evaluated. Another commercial insecurity is that these materials have late biocompatibility, particularly at low stimulation of the implant surface with the bone cells (osteoblasts) [10]. It is known that low concentrations of cationic elements, such as Mg^{2+}, can stimulate certain biological processes, such as cell adhesion and osteogenic differentiation [11,12]. Thus, this work aimed to evaluate the influence of low Mg concentration on the microstructural and mechanical properties of the Ti—34Nb—6Sn alloy, using the powder metallurgy technique.

2.   Experimental procedure

The amounts of TiH (ASTM F67), NbH (CBMM/Araxá-MG-Brasil) and atomized Sn (Metalpó/São Paulo-Brasil, 99.99%) to provide an alloy with a mass ratio of 60:34:6 of Ti, Nb and Sn, mixed and ground in a planetary ball mill (FRITZCH Pulverisette 5 model) under the following conditions: steel bottles with a capacity of 450 ml, steel balls with a radius between 3 mm and 2 mm and ethyl alcohol enough to cover the powders as a dispersant and to prevent heating. The powder mixture was ground at 200 rpm for 40 min and dried under vacuum. The Mg powder, when used, was equivalent to 3% in mass. According to some authors, the levels of Nb close to 30% by mass and the low content of Sn (up to 10%) can promote the decrease of the elastic modulus without affect the mechanical properties [13,14].

The dry powders were compacted at 200 MPa for 15 s. Sintering was carried out in a high vacuum resistive furnace (COMBUSTOL - tube furnace model) coupled to mechanical pumps and diffusers (Edwards). The sample chamber was pre-purged with argon at 450 °C, for 2 h to eliminate the PCA, followed by sintering at 900 °C and 1100 °C, for 2 h under vacuum (seen in Table 1 and Fig. 1).

For the embedding was used a transparent resin (Trans-Optic, Bhuler) at 180 °C for 3.5 min of heating, with a 350-bar pressure and 6 min for heating and cooling with water. A metallographic process was carried out to eliminate irregularities and surface oxides formed during the sintering process. This process was carried out at 150 rpm on a metallographic sander (Struers-Labopol-25), using a sequence of 80, 220, 500 and 1000 mesh SiC papers, always in water to avoid overheating and optimize the procedure time. Then were polished (Struers-Labopol-5) with a 9 μm solution (Dia-Maxx) at 200 rpm, followed by final OPS solution (Struers) and hydrogen peroxide (Derra) (10:2). Finally, the samples were clean with distilled water (18.2 MΩ cm) and ethyl alcohol/ acetone for 60 min in an ultrasound (Elma S30 H).

The particle size powders has been carried out by Dynamic Image Analyzer (Particle Insight-2.55-Shimadzu).

For the characterization and quantification of the current phases, as well as the lattice parameters of the structures, was used X-ray diffraction (Bruker/D2Phaser). A Cu Kα radiation was use that works at 30 kV and 10 mA. The measurement was made in the range of angles between 20 and 90°, with a step of 0.02° every 10 s. The refinement of the structure and the quantitative phase analysis were carried out using the free MAUD software (version 2.94).

The microstructure was characterized by Field Emission Scanning Electron Microscopy (FESEM) (ZEISS-ULTRA 55) with backscattered electrons (BSE), secondary electrons (SE) and X-ray energy dispersive detectors (EDS) (Oxford Instruments Ltda.).

The elastic modulus, E (GPa), was evaluated using the impulse excitation technique (ATCP, Sonelastic®). The hardness

Table 1 — Description of the conditions used for the Ti—Nb—Sn alloys synthesis.

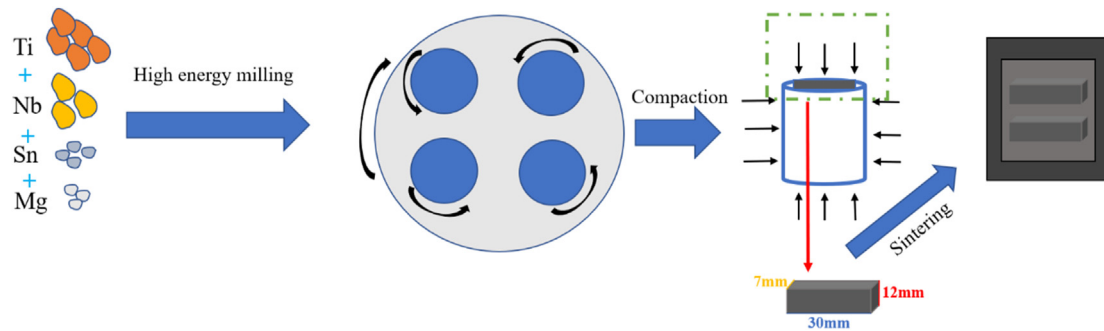| Material	Compaction (MPa)	Sintering process (°C)	Nomenclature
Ti—34Nb —6Sn	200	900	TNS_{900}
Ti—34Nb —6Sn/Mg	200	900	TNS/M_{900}
Ti—34Nb —6Sn	200	1100	TNS_{1100}
Ti—34Nb —6Sn/Mg	200	1100	TNS/M_{1100}

Fig. 1 − Scheme illustration of procedure fabrication of alloys.

was obtain using a load of 147 N by the Rockwell method (BECLA), with a spherical steel indenter of 1/16" diameter.

3. Results and discussion

3.1. Morphology and size powders evaluation

By analyzing the particle size, the TiH, NbH and Sn powders showed an average size approximately close, in a range from 17 to 18 μm approximately before milling, as can be seen in Table 2. In addition, the particles with maximum and minimum size of each element also presented close sizes, as well as D_{10}, D_{50} and D_{90}. After milling, the mixture had an average size of 5.8 ± 2.6 μm and 90% of the particles were approximately 9 μm (D_{90}). The TiH and NbH particles showed close circularity, while Sn particles showed less circularity. After milling, the circularity of the particles has a greater normal distribution with an average circularity of approximately 65% (seen in Table 2).

3.2. Microstructure characteristics

Fig. 2 shows the diffractogram of the TNS$_{900}$ and TNS$_{1100}$ systems. As can be seen two phases are present in all diffractograms. They are hexagonal compact (hcp), α phase and cubic of centered body (bcc), β phase. β-Ti as well as Nb crystalize in the W-type structure in the space group Im-3m, with slight difference in lattice parameters ($a_{\beta\text{-Ti}}$ = 3.327 Å and a_{Nb} = 3.305 Å); therefore, it is difficult to distinguish them using XRD technique [15,16]. The peak intensity of the {002}$_\alpha$ plane decreased its intensity about 20% (negative displacement). The peak intensity of the {110}$_\beta$ plane showed a significant increasing from 900 °C to 1100 °C about 18% with an angular negative displacement from 38.74° to 38.56°, as well as the peak of the {101}$_\alpha$ plane increased about 22% from 40.02° to 39.83° also with negative displacement.

The diffractograms of the TNS/M$_{900}$ and TNS/M$_{1100}$ systems (Fig. 3) also there was no detection of oxides, nitrides or intermetallic peaks. Only two phases were detected, being α and β phases. The peak intensity of the {002}$_\alpha$ plane decreased it about 9% with negative displacement. The peak of {110}$_\beta$ plane showed a significant increasing about 34% with an angular displacement from 38.65° to 38.61° and the peak of the {101}$_\alpha$ plane decrease it about 31% from 39.93° to 39.83° both negative displacements. The phase transformation occurred in all cases but more significative in TNS/M system (Table 3).

The increase in peak intensity related to the β phase may be due to the diffusion stage controlled by Ti. As the peak distribution intensity for the {110}$_\beta$ plane shows a greater increase than in the TNS system, it may be due to the lower diffusion rate of the Nb particles. As the difference between the Nb and Ti-β lattice parameters is very small, this increase is possibly due to the presence of Nb particles that have not been dissolved. According to Divinski et al., in the Ti−54Al−10Nb system the Nb diffusion coefficient was 3 times higher from 909.85 °C to 1164,85 °C [17].

It is known that during the heating process and the initial isothermal sintering, the densification of Ti and Nb alloys occurs mainly by self-diffusion between the Ti particles due to their greater diffusivity. The Nb particles, on the other hand, act at this stage as diffusion barriers for the Ti mass flow. The second diffusion stage, between Ti−Nb, sufficient strangulation occurs between the Ti and Nb particles to facilitate the mass transfer between the matrix of Ti and Nb particles, resulting in greater densification and/or to the matrix diffusion stage (in the final sintering phase, the bimodal structure of Ti−Nb transitions to a chemically heterogeneous Ti−Nb matrix that, as occurs subsequent diffusion, approaches a compositional homogeneity [18]. In addition, it should promote greater deformation in the structure, observed by the displacements of the peaks at 1100 °C. In the TNS/M system, the intensity of both peaks increased, however, they showed a smaller increase, compared to TNS, demonstrating that the

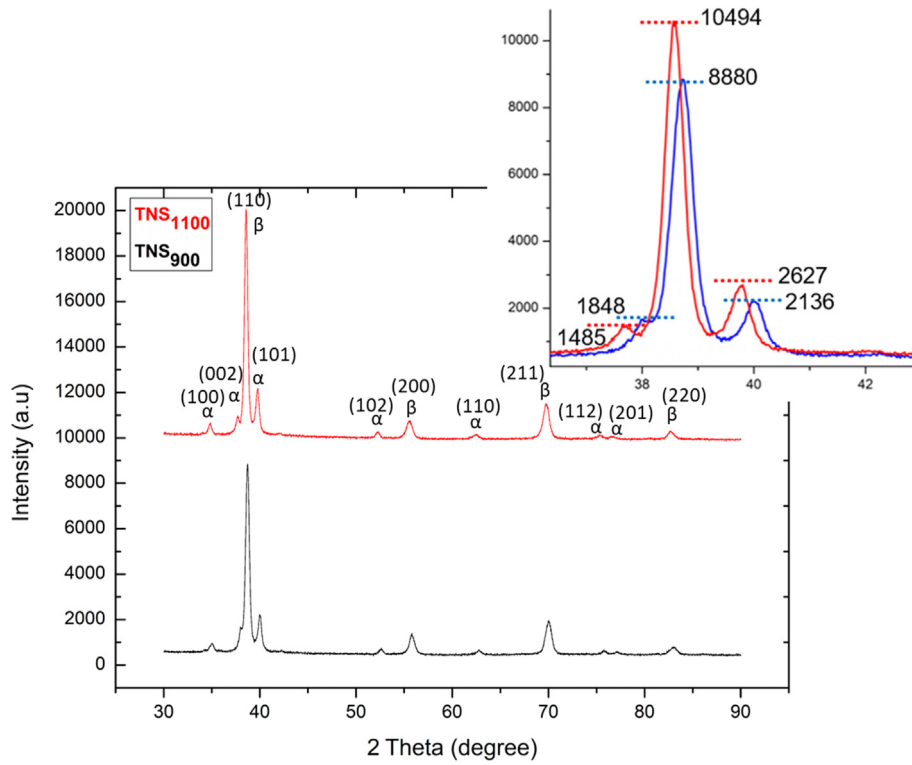| Table 2 − Particle size and circularity distribution by DIA.							
Elements	Maximum	Minimum	Mean ± SD	D_{10}	D_{50}	D_{90}	Circularity
Hydrated Titanium	140.7	5.8	17.4±10.7	8.5	14.2	30.5	0.60±0.1
Hydrated Niobium	199.0	5.6	18.3±12.0	8.6	14.6	32.6	0.59±0.1
Tin	107.2	5.7	17.1±8.8	9.0	14.6	28.5	0.63±0.1
Powders milled	24.1	3.0	5.8±2.6	3.4	5.1	9.3	0.65±0.1

Fig. 2 — XRD of TNS sintered materials.

magnesium particle may have increased the resistance to diffusion during the sintering process [19], promoting less deformation in the structure. The smaller increase can be confirmed by the lattice parameter variation of the bcc structure (Δa) it was 8.1 pm for TNS and 4.7 pm for TNS/M basically 2 times higher in TNS system. Some studies like
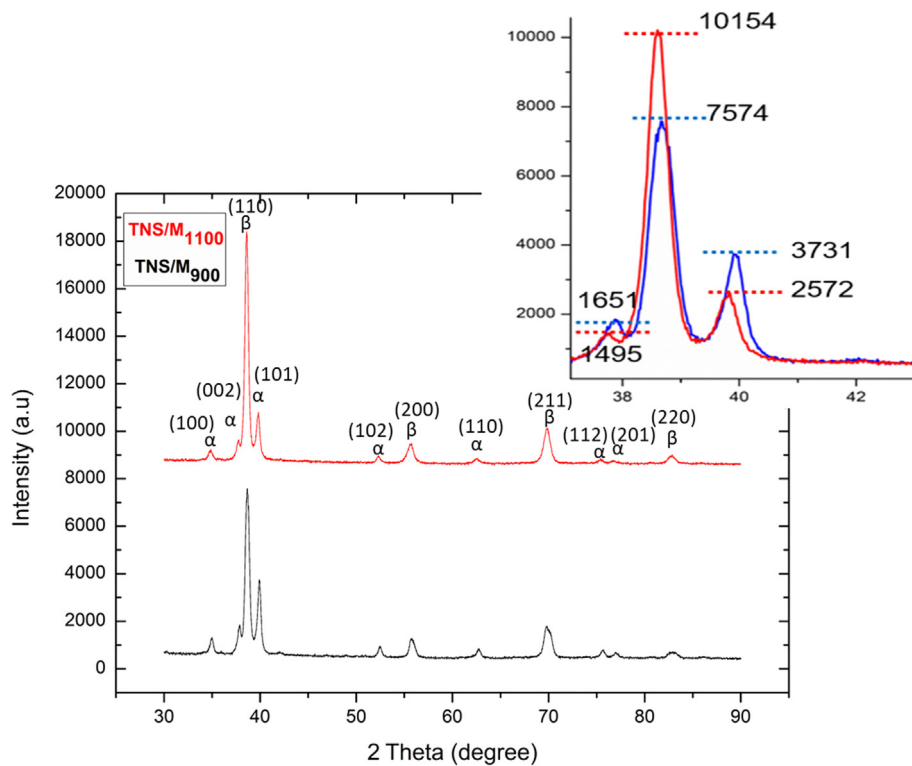

Fig. 3 — XRD of TNS/M sintered materials.

Table 3 – Quality factor, and % phases of sintered TNS and TNS/M materials.

Parameters	TNS_{900}	TNS_{1100}	TNS/M_{900}	TNS/M_{1100}
α (%)	20.1±0.3	23.8±0.5	35.3±0.0	22.4±0.0
β (%)	79.9±0.0	76.1±0.0	64.7±0.0	77.6±1.4
Rwp (%)	3.89	8.79	7.16	6.62

Table 4 – Experimental wt % of the elements by EDS detector.

Conditions	Ti (%)	Nb (%)	Sn (%)
TNS_{900}	62	32	6
TNS/M_{1100}	60	34	6
TNS_{1100}	60	34	6
TNS/M_{1100}	61	33	6
Nominal	60	34	6

Horiuchi et al., which evaluated the phase constitution of Ti-18 mol%Nb alloys containing 3 mol% of ternary elements, and indicated that the variation in the intensity distribution in XRD, as well as the deformation of the structure, is due to the addition of a ternary element [20].

The quality parameter of the Rwp refinement (%) was satisfactory in all cases (<10%). To compare TNS with TNS/M there was positive phase transformation in same sintering temperature (2% of the β phase transformation increment from TNS_{1100} to TNS/M_{1100}). At 900 °C there was a negative increment of the β phase transformation. It was TNS_{900} to TNS/M_{900} with 19% of the increment of β phase transformation. This way, the effect with magnesium addition when increase the sintering temperature is not significant to β→α transformation.

The constituent elements of the sintered systems had a content close to the nominal (seen in Table 4), indicating good homogeneity of the powders after milling. In Fig. 4 the microstructure is represented by the SEM analysis shows regions with different contrasts and pores formed with irregular type morphology. In the TNS system (Fig. 4A), at 900 °C, there is a greater presence of porosity and the microstructure is less homogeneous compare to 1100 °C (Fig. 4B). The porosity formation can be due to the incomplete sintering process, being more significant in the TNS/M system (Fig. 4C and D), corroborated also by the influence of the magnesium particles, increasing the resistance to diffusion. Note the presence of Nb particles (brightest contrast) that were not diffuse in the Ti lattice (Fig. 4A, C and D). Darkest contrast region, referring to α phase and intermediate contrast region, referring to β phase in all systems. The point analysis in Fig. 4C confirmed the presence of Nb particles with 98wt%, α phase with 93 wt% and β phase, more homogeneous region with wt% closer to the nominal. At 1100 °C, the structure presents more refined grain contours and a homogeneous microstructure it can be seen as evidenced by the low presence of non-diffused Nb particles (Fig. 4B and D).

In addition, there is a transgranular growth in needle forms, seen in Fig. 4B and D, possibly α secondary and discontinuous precipitation in grain limits. In the TNS/M system, there is also a microstructural evolution from 900 °C to 1100 °C systems, due to the significant diffusion of Nb particles (Fig. 4C and D). The microstructure of the TNS/M_{900} system is less refined compare to TNS_{900} system. Besides that, compare the TNS_{1100}, to TNS/M_{1100} it is less refined, due to elevate presence of Nb particles and there is a greater presence of darkest contrast regions referring to α phase, again indicating the resistance of the Nb particles diffusion, produced by the presence of magnesium particles.

In Figs. 5 and 6 is presented by the line analysis the Nb and Sn content in the microstructure at 1100 °C in both systems TNS and TNS/M. The regions indicated by the numbers 1, 3 and 5 presents homogeneous Nb and Sn content. The transition to regions 2 and 4 both Nb and Sn decrease content, where is present the high Ti content, referring to α1. In the microstructure represented by the number 6 the Nb content is low but the Sn is more dissolved.

The region indicated by the number 7 presents elevated concentration of Sn (darkest contrast), confirming its diffusion in Ti. The regions indicated by the number 8,9, 10 and 12 present higher homogeneity, due to linear alloy elements distribution. The 10 → 11→12 transition occurs abruptly due to the low diffusion process around the Nb particle [17]. The composition profile by mapping analysis of TNS and TNS/M are described in Figs. 7 and 8. In Fig. 7 there is the presence of insoluble Nb particles and Ti particles that have not been self-diffused on the microstructure. Further there are no Nb particles and Ti is more widespread due to the α→β allotropic transformation process. In addition, α secondary is noted around the grain boundaries. The Sn is presents well distributed and dissolved in the Ti microstructure except where are the Nb unsolved particles and determined regions of the α primary, confirmed by the line analysis of Figs. 5 and 6.

The porosity formation is two times greater than in the TNS system (seen in Table 5). The increase in porosity in the TNS/M system may be due to the presence of magnesium at the beginning of the sintering process, which due to the formation of the oxide layer, with increasing temperature, the gas is released forming pores [21]. In addition, with the increase in sintering temperature from 900 °C to 1100 °C, a decrease in porosity is observed, indicating greater densification and diffusion of the alloy elements. In Fig. 8, there are Nb particles precipitates and also Ti particles non-diffused. Magnesium is present in the richest regions in Nb and Sn and also around some pores. In addition, Sn is less widespread than in the TNS_{900} system (Fig. 7).

3.3. Mechanical properties

Fig. 9 shows the elastic modulus (E) of the TNS and TNS/M$_{900-1100}$ systems. There was a significant decrease it compares TNS/M→TNS system in both sintering processes. Besides that, TNS and TNS/M system increased significantly with the increase sintering temperature. The low E in all systems is due to the presence of a high concentration of β phase stabilizator element (Nb> 30%). In addition, due to the high porosity
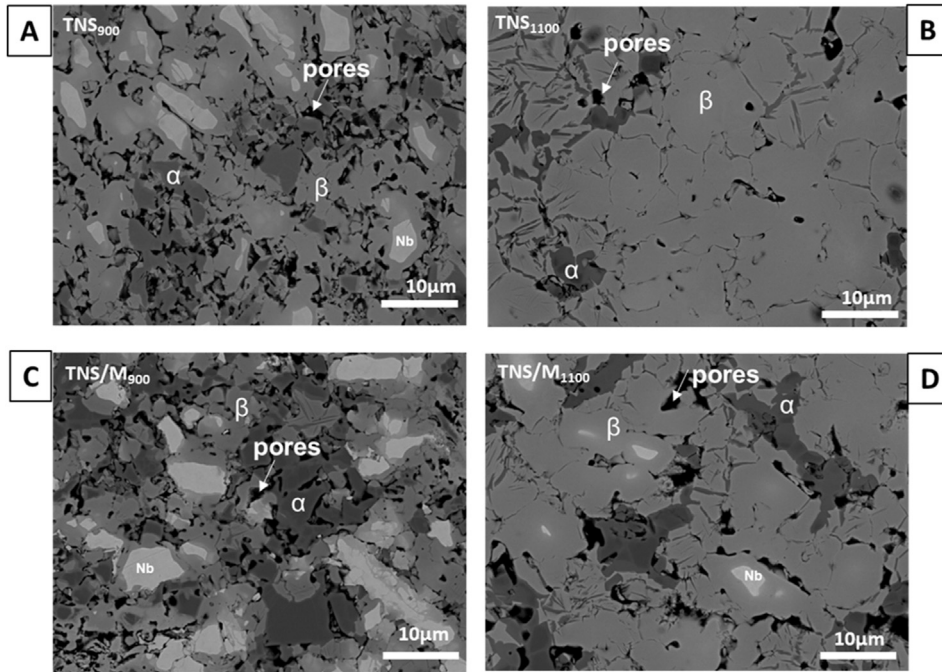
Region	Ti (wt%)	Nb (wt %)	Sn (wt %)
Darkest	96	-	4
Brightest	2	98	-
Intermediate	58	38	4

Fig. 4 − SEM of TNS and TNS/M materials using a BSE detector. All images were obtained with a 1000x of magnification.
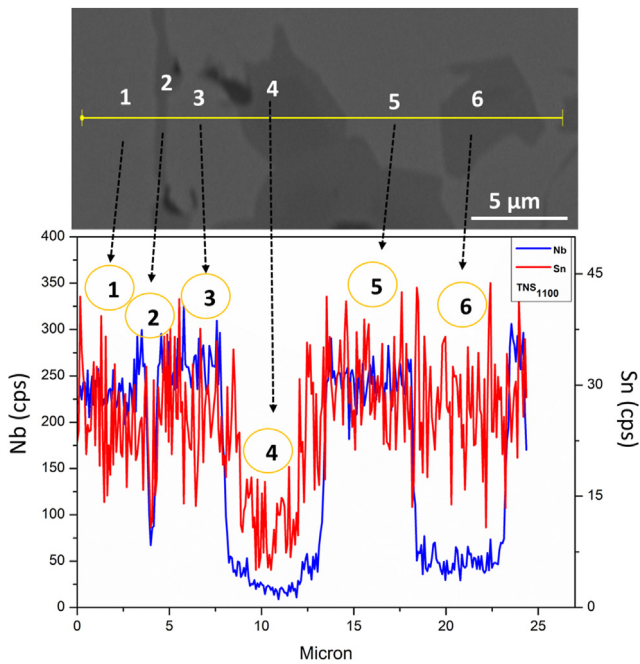

Fig. 5 − Nb and Sn distribution by line analysis of TNS using BSE detector. All images were obtained with a 2500x of magnification.

present, it may have contributed to the decrease it, even more significantly in TNS/M due to the greater resistance to diffusion.

The hardness of the TNS/M→TNS system decreased significantly in all experimental conditions (Fig. 10). The strength (Str) of the TNS/M→TNS also decreasing significantly, but to elevate the temperature of the sintering, both systems present higher hardness and maximum hardness resistance (Fig. 10). The improvement in hardness and strength is due to the refinement of the grain size, of the Nb particles [7].

The % of Nb particles (brightest contrast) that did not diffuse is 8% for TNS and 23% for TNS/M in the first sintering process (900 °C). After elevate the temperature (1100 °C), the presence of precipitated Nb particles in TNS/M is around 2% and in TNS they were not found. Besides that, the oxygen content detected was significant, in both systems, but in TNS/M it was 1.26 times higher, due to the magnesium presence (seen in Table 6 and Fig. 11). According to Nouri et al., the Ti−16Sn−4Nb alloy presented lower microhardness in milling time where the β phase transformation was more significative [7]. Even with the bcc low resistance to deformation compared to the hcp structure, the hardening increased, possible by the both conditions cited above.
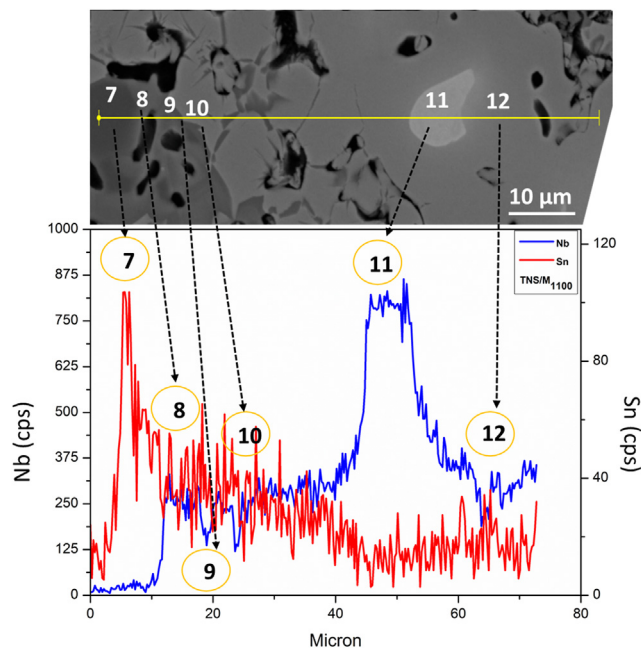
Fig. 6 – Nb and Sn distribution by line analysis of TNS/M using BSE detector. All images were obtained with a 2500x of magnification.

The hardness of Ti CP sintered at temperature, compaction pressure and similar grinding time, is 200 HV < Ti CP < 250 HV [22]. As well as similar alloys, such as 158 HV for Ti-33.6Nb4Sn [23] and 169 HV for Ti–30Nb–4Sn [24], which present oxygen content around 0.13 wt (%) and low hardness value compared to those developed in this present work. Even if there is no

concrete value that can serve as a reference for the selection of biomaterials, it is clear that at least these hardness values must be exceeded by those present, but it is not even possible to have the greatest possible hardness that is related to them. The mechanical properties could produce the bone resorption. The metals and alloys present a more homogeneous hardness, regardless of the direction of the strength, and this is related to its mechanical resistance, especially the compression, it must allow to distribute the strengths with the strength and accompaniment in its deformation (rigidity), provided by the elastic module. The Ti CP has a hardness of 220 H V while the Ti–6Al–4V alloy reaches 350 H V. In this case, the hardnesses that present in our alloys fluctuate between these two, because they are between 226 H V and 900 °C and 344 H V when sintered at 1100 °C. In relation to E, it is known that bone tissue presents a range between 0.5 and 20 GPa, depending on the type of bone (cortical or trabecular bone) [25]. In more detail, inside the femur, the elastic module at 11.7 GPa in radial and tangential directions, an 18.2 GPa in longitudinal direction. However, in the cancellous bone the moduli are 0.445 GPa in proximal tibia and 0.389 GPa in the femur. Similar behavior is observed in the maximum resistance to compression, with values of 0.00533 GPa in the proximal tibia and 0.00736 GPa in the femur, for the cancellous bone, although the fracture in the compression in the cortical bone is produced, in the femur, 0.205 GPa in longitudinal direction and 0.130 GPa in tangential direction, which would correspond approximately to 21 H V and 13 H V respectively [26].

Note that with the addition of magnesium, E decreases significantly, in the range of 30 GPa at 900 °C and 49 GPa at 1100 °C. Even with the decrease in hardness (226 H V at 900 °C
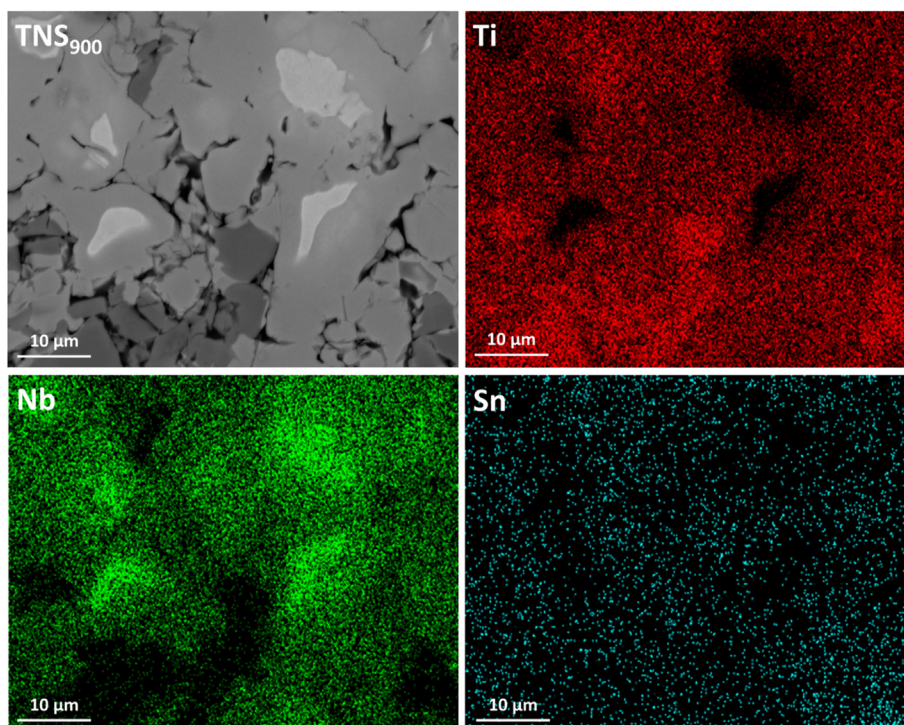

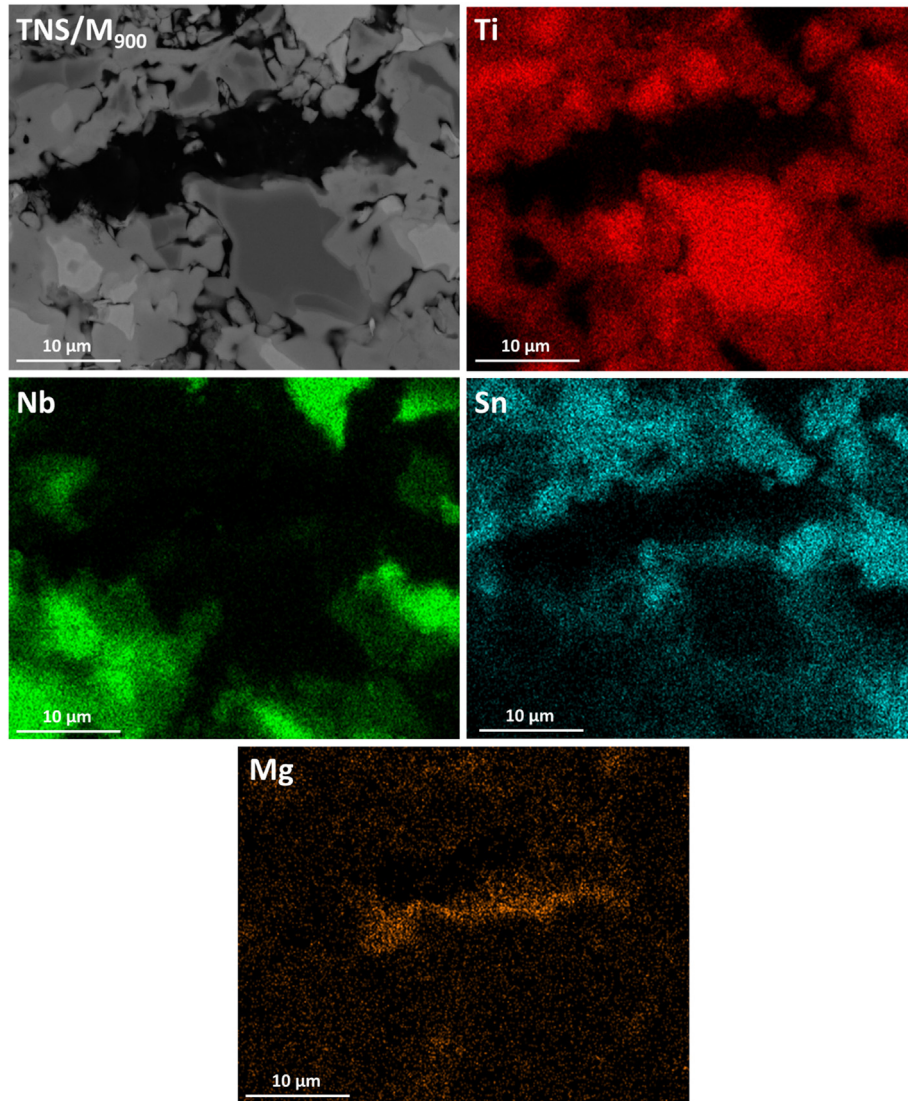**Fig. 7 – SEM-EDS elemental map analysis for the TNS alloy at 900 °C. Magnification of 2500x.**
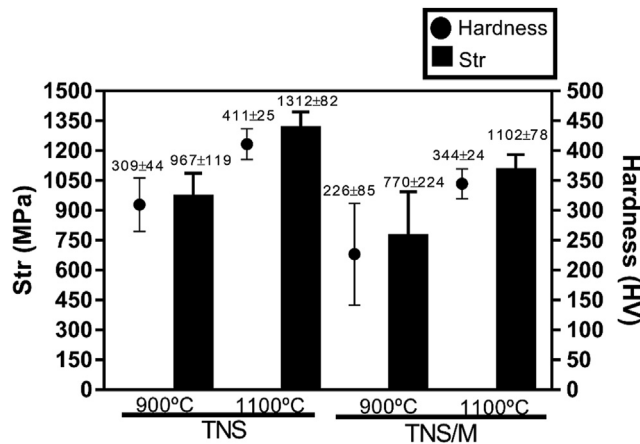
Fig. 8 – SEM-EDS elemental map analysis for the TNS/M alloy at 900 °C. Magnification of 2500x.

Table 5 — Pore characterization from software Image Tool (2D-analysis) and Archimedes'principle (3D-analysis).
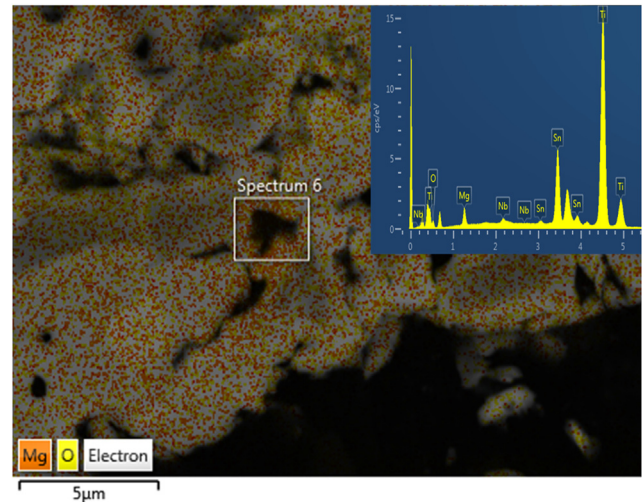
Materials	% Total Porosity by Image Analyzer	% Total Porosity by Archimedes
TNS_{900}	13 ± 2	22 ± 1
TNS_{1100}	$5.2\pm.1$	11 ± 1
TNS/M_{900}	26 ± 3	29 ± 1
TNS/M_{1100}	11 ± 1	20 ± 0.5
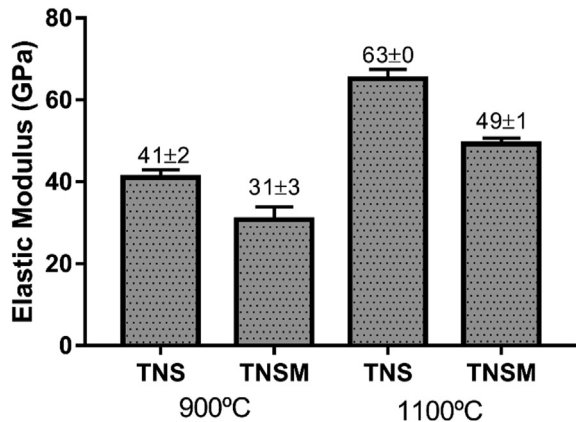
Fig. 9 — Elastic modulus by impulse excitation technique of the sintered materials.

Fig. 11 — EDS elemental map analysis and Mg and O distribution on the TNS/M alloy.

Fig. 10 — Hardness and Maximum strength evaluation by Vickers in sintered materials.

4. Conclusion

In this work, the microstructure and mechanical properties of the Ti—34Nb—6Sn/Mg alloys fabricated by elemental powder metallurgy sintering at 900—1100 °C are investigated. The conclusions are drawn as follows:

i. It is feasible the fabrication of the Ti—34Nb—6Sn/Mg alloys from the blended powders via step sintering at 900 °C/2 h and 1100 °C/2 h;

ii. Sintering temperature present essential effect on the Nb particles diffusion;

iii. It is clear that the magnesium difficult the sinterability of the Ti—34Nb—6Sn, and increase the wt% of the oxygen present in the samples;

iv. The porosity was 2 times higher on the Ti—34Nb—6Sn/Mg compared to Ti—34Nb—6Sn; Besides that, the porosity at 900 °C was around 30% and at 1100 °C 20% on the system with Mg, contributing for the decreasing of the elastic modulus;

v. The elastic moduli and hardness decreased significantly in Ti—34Nb6Sn/Mg around of 31 GPa and 226 H V at 900 °C and 49 GPa and 344 H V at 1100 °C.

Declaration of Competing Interest

The authors declare that they have no known competing financial interests or personal relationships that could have appeared to influence the work reported in this paper.

and 344 H V at 1100 °C) and resistance (770 MPa at 900 °C and 1102 MPa at 1100 °C), the values found are close to materials with similar chemical composition, such as Ti—30Nb—5Sn [8] and also higher than materials already used commercially, such as 102 GPa for TiCP grade 2 [27] and 110 GPa for Ti—6Al—4V [28].

Table 6 — Oxygen and nitrogen content.

Material	O (%)	N (%)
TNS_{1100}	1.030	0.117
TNS/M_{1100}	1.300	0.141

REFERENCES

[1] Report Buyer (July 2020). reportGlobal orthopedic prosthetic implants industry. Report ID: 544359. https://www.reportbuyer.com/product/5443591/global-orthopedic-prosthetic-implants-industry.html.

[2] Miura K, Yamada N, Hanada S, Jung T-K, Itoi E. The bone tissue compatibility of a new Ti–Nb–Sn alloy with a low Young's modulus. Acta Biomater 2011;7(5):2320–6. https://doi.org/10.1016/j.actbio.2011.02.008.

[3] Matsumoto H, Watanabe S, Hanada S. Beta TiNbSn alloys with low Young's modulus and high strength. Mater Trans 2005;46:1070–8. https://doi.org/10.2320/matertrans.46.1070.

[4] Okazaki Y, Rao S, Tateishi T, Ito Y. Cytocompatibility of various metal and development of new titanium alloys for medical implants. Mater Sci Eng, A 1998;243(1–2):250–6. https://doi.org/10.1016/s0921-5093(97)00809-5.

[5] Banerjee D, Williams JC. Perspectives on titanium science and technology. Acta Mater 2013;61(3):844–79. https://doi.org/10.1016/j.actamat.2012.10.043.

[6] Mahran GMA, Omran A-NM. Fabrication of a β Ti–30Nb–4Sn biomedical alloy using mechanical alloying. Sci Adv Mater 2018;10(10):1509–18. https://doi.org/10.1166/sam.2018.3352.

[7] Nouri A, Chen X, Li Y, Yamada Y, Hodgson PD, Wen C. Synthesis of Ti–Sn–Nb alloy by powder metallurgy. Mater Sci Eng, A 2008;485(1–2):562–70. https://doi.org/10.1016/j.msea.2007.10.010.

[8] Adiningsih DR, Utomo EP, Anawati Inicial. The microstructure and mechanical hardness of cast Ti-30Nb-5Sn after solution treatment. IOP Conf Ser Mater Sci Eng 2019;541(1):012049. https://doi.org/10.1088/1757-899X/541/1/012049.

[9] Sharma B, Vajpai SK, Ameyama K. Synthesis of ternary Ti-25Nb-11Sn alloy by powder metallurgy route using titanium hydride powder. Mater Trans 2016;57(9):1440–6. https://doi.org/10.2320/matertrans.MH201510.

[10] Oron A, Agar G, Oron U, Stein A. Correlation between rate of bony ingrowth to stainless steel, pure titanium, and titanium alloy implants in vivo and formation of hydroxyapatite on their surfaces in vitro. J Biomed Mater Res 2009;91(4):1006–9. https://doi.org/10.1002/jbm.a.32299.

[11] Wang J, Ma X-Y, Feng Y-F, Ma Z-S, Ma T-C, Zhang Y, et al. Magnesium ions promote the biological behaviour of rat calvarial osteoblasts by activating the PI3K/akt signalling pathway. Biol Trace Elem Res 2017;179(2):284–93. https://doi.org/10.1007/s12011-017-0948-8.

[12] Nie X, Sun X, Wang C, Yang J. Effect of magnesium ions/Type I collagen promote the biological behavior of osteoblasts and its mechanism. Regen Biomater 2020;7(1):53–61. https://doi.org/10.1093/rb/rbz033.

[13] Ozaki T, Matsumoto H, Watanabe S, Hanada S. Beta Ti alloys with low Young's Modulus. Mater Trans 2004;45(8):2776–9. https://doi.org/10.2320/matertrans.46.1070.

[14] Cremasco A, Osório WR, Freire CMA, Garcia A, Caram R. Electrochemical corrosion behavior of a Ti–35Nb alloy for medical prostheses. Electrochim Acta 2008;53(14):4867–74. https://doi.org/10.1016/j.electacta.2008.02.011.

[15] Massalski TB. Binary alloy phase diagrams, vol. 2. Cleveland, Ohio, USA: American Society for Metals; 1986.

[16] Salvo C, Aguilar C, Cardoso-Gil R, Medina A, Bejar L, Mangalaraja RV. Study on the microstructural evolution of Ti-Nb based alloy obtained by high-energy ball milling. J Alloys Compd 2017;720:254–63. https://doi.org/10.1016/j.jallcom.2017.05.262.

[17] Divinski S, Hisker F, Klinkenberg C, Herzig C. Niobium and titanium diffusion in the high niobium-containing Ti–54Al–10Nb alloy. Intermetallics 2006;14(7):792–9. https://doi.org/10.1016/j.intermet.2005.12.007.

[18] Zhao D, Chang K, Ebel T, Nie H, Willumeit R, Pyczak F. Sintering behavior and mechanical properties of a metal injection molded Ti–Nb binary alloy as biomaterial. J Alloys Compd 2015;640:393–400. https://doi.org/.

[19] Alias J, Harun WSW, Ayu HM. Review on the preparation of magnesium-based alloys prepared by powder metallurgy and the evolution of microstructure and mechanical properties. Key Eng Mater 2019;796:3–10. https://doi.org/10.4028/www.scientific.net/KEM.796.3.

[20] Horiuchi Y, Inamura T, Kim HY, Miyazaki S, Wakashima K, Hosoda H. X-ray diffraction analysis of Ti-18 mol%Nb based shape memory alloys containing 3d transition metal elements. Mater Trans 2006;47(4):1209–13. https://doi.org/10.2320/matertrans.47.1209.

[21] Burke P, Kipouros GJ, Fancelli D, Laverdiere V. Sintering fundamentals of Mg powders. Can Metall Q 2009;48(2):123–32. https://doi.org/10.1179/cmq.2009.48.2.123.

[22] Singh P, Abhash A, Yadav BN, Shafeeq M, Singh IB, Mondal DP. Effect of milling time on powder characteristics and mechanical performance of Ti4wt%Al alloy. Powder Technol 2019;342:275–87. https://doi.org/10.1016/j.powtec.2018.09.075.

[23] Salvador CAF, Lopes ESN, Ospina CA, Caram R. Orthorhombic martensite formation upon aging in a Ti-30Nb-4Sn alloy. Mater Chem Phys 2016;183:238–46. https://doi.org/10.1016/j.matchemphys.2016.08.023.

[24] Salvador CAF, Opini VC, Lopes ESN, Caram R. Microstructure evolution of Ti–30Nb–(4Sn) alloys during classical and step-quench aging heat treatments. Material Sci Technol 2017;33(4):400–7. https://doi.org/10.1080/02670836.2016.1216030.

[25] Gibson LJ. The mechanical behaviour of cancellous bone. J Biomech 1985;18(5):317–28. https://doi.org/10.1016/0021-9290(85)90287-8.

[26] Murphy W, Black J, Hastings G, editors. Handbook of Biomateria lProperties, seconded. NewYork: Springer-Verlag; 2016. https://doi.org/10.1007/978-1-4939-3305-1.

[27] Niinomi M. Mechanical properties of biomedical titanium alloys. Mater Sci Eng, A 1998;243(1–2):231–6. https://doi.org/10.1016/s0921-5093(97)00806-x.

[28] Niinomi M, Liu Y, Nakai M, Liu H, Li H. Biomedical titanium alloys with Young's moduli close to that of cortical bone. Regen Biomater 2016;3(3):173–85. https://doi.org/10.1093/RB/RBW016.